The Astrophysical Journal Letters, 765:L18 (6pp), 2013 March 1 doi:10.1088/2041-8205/765/1/L18

COSMIC RAY MODULATION BEYOND THE HELIOPAUSE: A HYBRID MODELING APPROACH

R. D. Strauss[1], M. S. Potgieter[1], S. E. S. Ferreira[1], H. Fichtner[2], and K. Scherer[2]
[1] Centre for Space Research, North-West University, Potchefstroom Campus, Private Bag X6001, Potchefstroom 2520, South Africa; dutoit.strauss@nwu.ac.za
[2] Institut für Theoretische Physik, Lehrstuhl IV: Weltraum- und Astrophysik, Ruhr-Universität Bochum, D-44780 Bochum, Germany
Received 2012 December 13; accepted 2013 February 1; published 2013 February 15

ABSTRACT

Results from a newly developed hybrid cosmic ray (CR) modulation model are presented. In this approach, the transport of CRs is computed by incorporating the plasma flow from a magnetohydrodynamic model for the heliospheric environment, resulting in representative CR transport. The model is applied to the modulation of CRs beyond the heliopause (HP) and we show that (1) CR modulation persists beyond the HP, so it is unlikely that the *Voyager* spacecraft will measure the pristine local interstellar spectra of galactic CRs when crossing the HP. (2) CR modulation in the outer heliosheath could maintain solar-cycle-related changes. (3) The modulation of CRs in the outer heliosheath is primarily determined by the ratio of perpendicular to parallel diffusion, so that the value of the individual diffusion coefficients cannot be determined uniquely using this approach. (4) CRs can efficiently diffuse between the nose and tail regions of the heliosphere.

Key words: astroparticle physics – cosmic rays – magnetohydrodynamics (MHD) – methods: numerical – Sun: heliosphere

Online-only material: color figures

1. INTRODUCTION

The *Voyager 1* (*V1*) spacecraft will cross the heliopause (HP) in the near future and sample, for the first time, the interstellar medium (ISM) in situ. Some evidence from particle observations suggest that *V1* may have already crossed the HP (e.g., Webber et al. 2012), although some authors, e.g., McComas & Schwadron (2012), dispute this claim. Although the HP separates the solar wind and interstellar plasmas, the Sun's influence extends beyond the HP by disturbing the ISM upstream of the HP, forming the outer heliosheath. Recently, Scherer et al. (2011) have shown that galactic cosmic ray (CR) modulation could also extend well into the outer heliosheath (see also Herbst et al. 2012). The consequence is that *V1* may not measure the pristine local interstellar spectrum (LIS) of galactic CRs at the HP, but would rather continue to measure a positive CR gradient well beyond the HP. We further investigate this topic by introducing and applying a newly developed hybrid CR transport model. In this approach, the relevant CR transport equation (TPE) is solved using a magnetohydrodynamic (MHD) simulated heliosphere and a disturbed local ISM. In generalization to the model used by Scherer et al. (2011), we present a representative modeling scenario by (1) computing, instead of assuming, a heliospheric geometry, including a termination shock (TS), (2) introducing subsequently credible plasma flow fields, including a non-radial solar wind flow and a non-Parkerian heliospheric magnetic field (HMF) beyond the TS region, and (3) also including the effects of the interstellar magnetic field (ISMF) which were not considered by Scherer et al. (2011).

2. A HYBRID CR MODULATION MODEL

2.1. The MHD Model

It should be noted that the focus of the present work is on CR transport and that, for this first approach, the *basic* MHD model used here is not meant to rival the more complex models of, e.g., Pogorelov et al. (2011). The main features of these more complex MHD models are, however, still reflected in the results from the simpler approach adopted here. The heliospheric geometry is obtained by solving the set of ideal MHD equations, given as (e.g., Landau & Lifshitz 1984)

$$\begin{aligned}
&\frac{\partial \rho}{\partial t} + \nabla \cdot (\rho \boldsymbol{u}) = 0\\
&\frac{\partial (\rho \boldsymbol{u})}{\partial t} + \nabla \cdot \left(\rho \boldsymbol{u} \otimes \boldsymbol{u} + p^{*}\mathbf{I} - \frac{1}{4\pi}\boldsymbol{B} \otimes \boldsymbol{B} \right) = 0\\
&\frac{\partial e}{\partial t} + \nabla \cdot \left[(e + p^{*})\boldsymbol{u} - \frac{1}{4\pi}\boldsymbol{B}(\boldsymbol{B} \cdot \boldsymbol{u}) \right] = 0\\
&\frac{\partial \boldsymbol{B}}{\partial t} - \nabla \times (\boldsymbol{u} \times \boldsymbol{B}) = 0. \qquad (1)
\end{aligned}$$

Here, $\boldsymbol{u}$ is the plasma flow velocity, ρ mass density, $\boldsymbol{B}$ magnetic field, $\mathbf{I}$ symbolized the identity matrix, $p^{*} = p + B^{2}/8\pi$ is introduced for shorter notation and the total energy is given by

$$e = \frac{\rho |\boldsymbol{u}|^{2}}{2} + \frac{p}{\gamma - 1} + \frac{B^{2}}{8\pi}. \qquad (2)$$

Closure is obtained by using the ideal gas law, relating thermal pressure p and temperature T by $p = 2nkT$, with thermal energy given by $\epsilon = p/(\gamma - 1)$, $\gamma = 5/3$ the ratio of specific heats for a mono-atomic proton gas and n the number density.

The MHD equations are solved by using the three-dimensional MHD solver of Pen et al. (2003). This well-documented MHD solver uses the total variation diminishing upwind scheme of Jin & Xin (1995) to advect the fluid variables, while constraint transport (Evans & Hawley 1988) is used to solve the magnetic field induction equation, thereby enforcing $\nabla \cdot \boldsymbol{B} = 0$. After initializing the MHD model, the projection scheme of Brackbill & Barnes (1980) is used to ensure a divergence-free initialization of $\boldsymbol{B}$. As an initial condition, a heliospheric inner boundary is specified within a radius of 50 AU from the Sun with a constant and radial solar wind with $|\boldsymbol{u}| = 400$ km s^{-1}, a Parker (1958) HMF normalized to

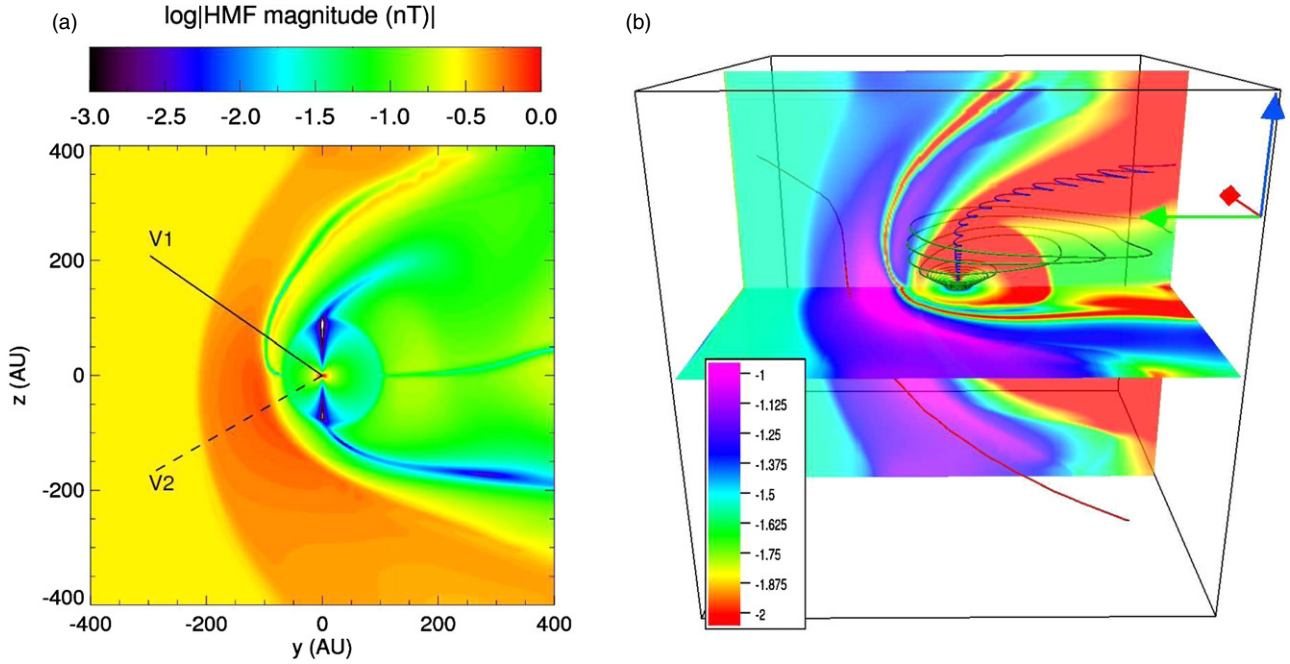

Figure 1. Left panel shows the modeled $|\boldsymbol{B}|$ in the meridional plane of the heliosphere as a contour plot. The ISM moves toward the right in the rest system of the Sun, located at the origin. The trajectories of the *Voyager 1* and *2* spacecraft are projected onto the same plane. The right panel shows contour plots of $|\boldsymbol{B}|$ (in arbitrary units on a logarithmic scale) in the meridional and ecliptic planes (note the inverted color scale), the spiralling green and blue lines show modeled HMF lines, and the red line shows an ISMF line.

(A color version of this figure is available in the online journal.)

5 nT at Earth, a proton number density of 5 particles cm^{-3} at Earth, decreasing as r^{-2}, and an adiabatic temperature decrease ($T \propto r^{-4/3}$), normalized to 10^5 K at Earth. The ISM is initialized with the parameters $|\boldsymbol{u}| = 26$ km s^{-1} (directed parallel to the HMF ecliptic plane), $T = 10^4$ K, $n = 0.2$ particles cm^{-3}, and $|\boldsymbol{B}| = 3$ μG. The ISM value of ρ, which is a factor $\sim$2 larger than consensus values, is chosen so that the additional kinetic pressure compresses the heliosphere to the approximate dimensions given by multi-fluid models (Müller et al. 2008). Recent studies have shown the influence of the ISMF (both in magnitude and directionality) on the modeled heliosphere, leading to various heliospheric asymmetries (e.g., Opher et al. 2006; Pogorelov et al. 2011). Here we assume the ISMF to be inclined 45° with respect to $\boldsymbol{u}$ (in both the meridional and ecliptic planes). This assumption is also in line with the inferred orientation of the ISMF as inferred through IBEX results (McComas et al. 2009; Schwadron et al. 2011).

Figure 1 shows the modeled heliospheric environment in terms of $|\boldsymbol{B}|$ in the meridional plane of the heliosphere. The resulting geometry is similar to that of Opher et al. (2006) and Pogorelov et al. (2007), with the ISMF compressing the heliosphere's southern hemisphere. As noted by Pogorelov et al. (2007), adopting an inclined ISMF (as is done in this study) results in a heliosphere without any plane of symmetry. The right panel of Figure 1 shows $|\boldsymbol{B}|$ in the meridional and ecliptic planes, the green and blue lines show two HMF lines, and the red line a single ISMF line. Note that the HMF becomes increasingly non-Parkerian outside the TS region.

2.2. The SDE-based CR Transport Model

The transport of CRs is described by the Parker (1965) TPE, given by

$$\frac{\partial f}{\partial t} = -\boldsymbol{u}\cdot\nabla f + \nabla\cdot(\mathbf{K}\cdot\nabla f) + \frac{1}{3}(\nabla\cdot\boldsymbol{u})\frac{\partial f}{\partial \ln P}, \quad (3)$$

in terms of the CR distribution function f, related to the CR differential intensity $j = P^2 f$ with P particle rigidity. Gradient and curvature drifts are not included because tests show that the effects thereof on CR intensities are negligible beyond the HP. We opt to solve Equation (3) by means of an Stochastic differential equation (SDE) based numerical model, transforming the TPE, which is a five-dimensional second-order partial differential equation, into a set of four first-order SDEs, given in Cartesian coordinates by (e.g., Gardiner 1983; Kloeden & Platen 1999; Kopp et al. 2012)

$$\begin{aligned} d\boldsymbol{x} &= (\nabla\cdot\mathbf{K} - \boldsymbol{u})\,ds + \mathbf{C}\cdot d\boldsymbol{w} \\ dP &= \frac{P}{3}(\nabla\cdot\boldsymbol{u})\,ds, \end{aligned} \quad (4)$$

where $2\mathbf{K} = \mathbf{C}\cdot\mathbf{C}^T$, $d\boldsymbol{w}$ is a multi-dimensional Wiener process and s is a time parameter. The methodology of integrating Equations (4) numerically is discussed by, e.g., Zhang (1999) and Strauss et al. (2011a). Essentially, Equations (4) describes the temporal evolution of a phase-space density element, which is integrated backward in time from an initial point $(\boldsymbol{x}^0, P^0)$ iteratively, e.g., $\boldsymbol{x}^{s+1} = \boldsymbol{x}^s + \Delta\boldsymbol{x}^s$, until a modulation boundary is reached where the LIS is specified. The modulation boundary for the present model is the outer boundary of the MHD simulation, which is a cube with a volume of (800 AU)^3. An important feature of the hybrid modeling approach is the coupling of the SDE model to the MHD generated heliospheric environment (see also Ball et al. 2005; Florinski & Pogorelov 2009). This is done by importing the quantities generated by the MHD model into the SDE model and solving for the CRs as test particles. The SDE approach is unable to produce global CR intensities at all energies in the heliosphere, and as such, the back-reaction of the CR pressure on the background plasma flow cannot be added self-consistently. As the MHD quantities are specified on a numerical grid, while the SDE model is essentially *grid-free*,

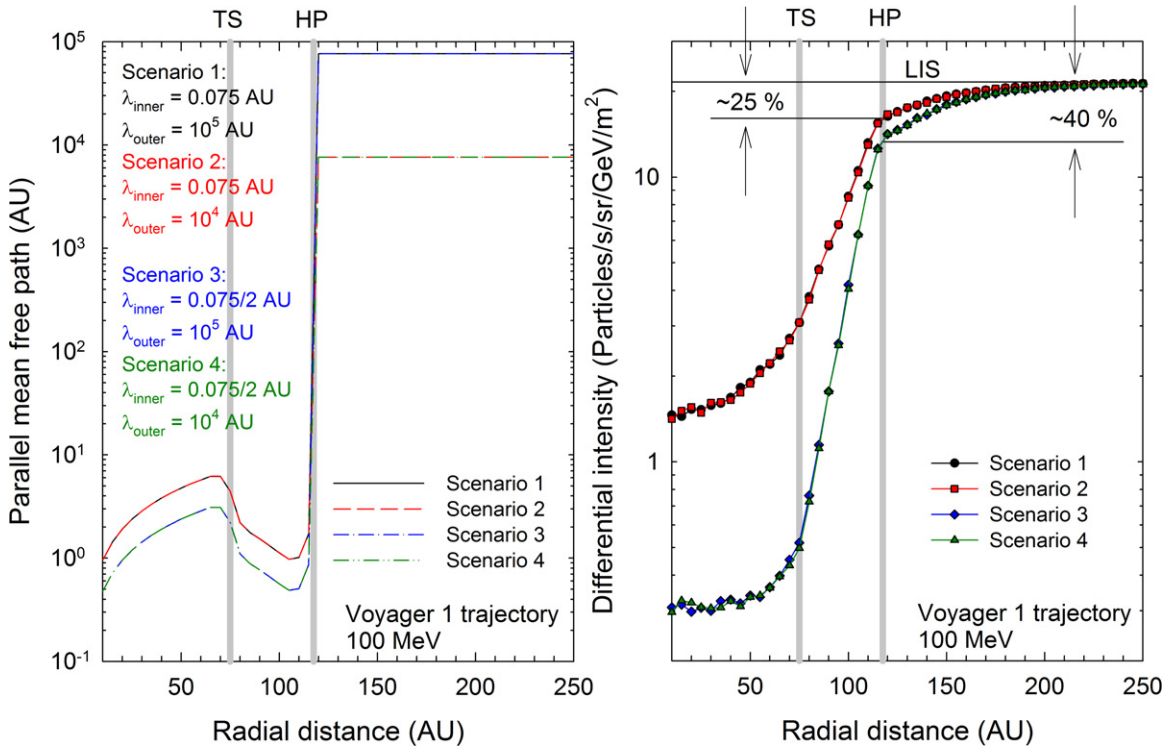

Figure 2. Left panel shows different assumptions of $\lambda_{||}$ at an energy of 100 MeV along the *V1* trajectory. The TS and HP positions are indicated by the vertical gray lines. The right panel shows the resulting CR proton differential intensity.

(A color version of this figure is available in the online journal.)

the MHD quantities are interpolated by a tri-linear interpolation to the present position of the pseudo-particles. Note that the diffusion tensor given in Equation (3) needs to be described in local (Cartesian) coordinates, although it is usually specified in terms of $\boldsymbol{B}$-aligned coordinates. The different diffusion tensors are related by

$$\mathbf{K} = \mathbf{A} \cdot \mathbf{K}^s \cdot \mathbf{A}^T, \tag{5}$$

where $\mathbf{A}$ is a rotation matrix (see, e.g., Effenberger et al. 2012) constructed from the MHD model output. For this work we assume the parallel mean free path to be given by

$$\lambda_{||} = \lambda_0 \frac{B_0}{|\boldsymbol{B}|} \left[\frac{P}{P_0} \right]^{\delta}, \tag{6}$$

with $P_0 = 1$ GV. The parameter δ determines the rigidity dependence of the diffusion process, with $\delta = 1$ if $P > P_0$, or else $\delta = 1/3$ (e.g., Teufel & Schlickeiser 2003). Similarly, B_0 is a constant with $B_0 = 5$ nT inside the HP, whereas, in the outer heliosheath, $B_0 = |\boldsymbol{B}|$, so that the diffusion coefficients have no spatial dependence in this region. For the perpendicular mean free path it is assumed that $\lambda_{\perp 1,2} = \eta \lambda_{||}$. The mean free paths are related to the diffusion coefficients through $\kappa_{xx} = \lambda_{xx} v/3$, with v the particle speed. Throughout this work, the proton LIS of Moskalenko et al. (2002) is specified as an outer boundary condition. An important constraint in the SDE model is the choice of the numerical time step Δs. Here,

$$\Delta s = \min \left\{ \frac{(1\ \mathrm{AU})}{|\max(\nabla \cdot \mathbf{K}, \boldsymbol{u})|}, \frac{(1\ \mathrm{AU})^2}{\max(\mathbf{K})} \right\}, \tag{7}$$

with $\max(\mathbf{K}) = \kappa_{||}$, ensuring that the pseudo-particles never (on average) propagate more than 1 AU in a single time step, thereby sampling the modeled heliosphere sufficiently. Moreover, the first term in this time constraint is needed to correctly simulate first-order Fermi (diffusive shock) acceleration occurring at the TS (Krülls & Achterberg 1994; Achterberg & Schure 2011).

3. MODELING RESULTS: CR MODULATION BEYOND THE HP

Results from the hybrid model are shown in Figure 2. The left panel shows the assumed $\lambda_{||}$ as a function of radial distance along the *V1* trajectory, while the right panel shows the resulting CR differential intensity at 100 MeV. The approximate positions of the TS and HP are indicated by the vertical gray lines. Results are shown for four scenarios of λ_0 as indicated on the figure, with $\eta = 0.02$. For scenario 1, $\lambda_0 = 0.075$ AU inside the heliosphere and $\lambda_0 = 10^5$ AU in the outer heliosheath. Note that $\lambda_0 = 10^5$ AU gives $\kappa_{||} \approx 1.5 \times 10^{28}$ cm^2 s^{-1}, an oftenly used value in galactic CR propagation models (e.g., Shalchi & Büsching 2010). The computed CR differential flux, corresponding to scenario 1 (black circles), shows three different modulation regions, characterized through the radial CR intensity gradient g_r: (1) upstream of the TS g_r is relatively small, (2) increasing significantly in the inner heliosheath, and (3) becoming small again in the outer heliosheath to eventually approach zero. Note that g_r is always positive. We thus confirm the results of Scherer et al. (2011), with a ~25% decrease in CR intensity in the outer heliosheath, while contradicting the earlier suggestion made by Jokipii (2001) that very little or no CR modulation should occur beyond the HP. It is, however, well known that galactic CR propagation models, producing as output the different LISs, do not take local ISM effects into account (e.g., Potgieter 2008). It is thus unlikely that *V1* will encounter the LIS just beyond the HP. Scenario 2 is similar to

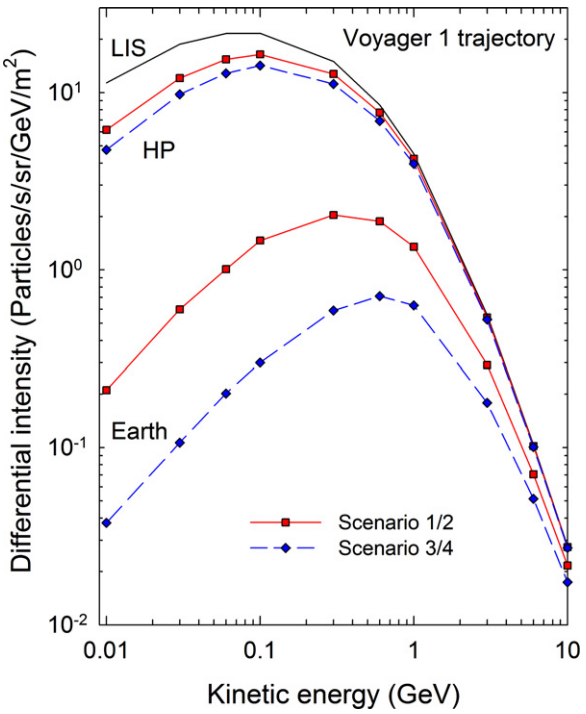

Figure 3. Computed CR proton energy spectra at the HP (top two colored curves) and at Earth (two bottom curves) with respect to the unmodulated LIS. The red and blue lines correspond to two different assumptions of $\lambda_{||}$ inside of the HP (see Figure 2) representing solar minimum and maximum modulation conditions.

(A color version of this figure is available in the online journal.)

scenario 1, except that $\lambda_0 = 10^4$ AU in the outer heliosheath. A striking result is that there is no change in the CR flux; CR modulation beyond the HP is therefore not determined by the value of the individual diffusion coefficients in this region. This effect is discussed further below. Scenarios 3 and 4 are similar to those previously described, with the value of λ_0 inside of the HP decreased by a factor of two, producing a large increase in modulation in all regions considered. This concurs with the conclusions made by Scherer et al. (2011): CRs are modulated in the outer heliosheath because of their mobility across the HP, entering and exiting the HP regions multiple times and cooled adiabatically while propagating in the supersonic solar wind regions. If increased modulation is experienced in the inner heliosheath, more modulation will also occur in the outer heliosheath.

In Figure 3 energy spectra are shown at Earth and at the HP for two choices of λ_0 inside the HP. The blue dashed lines correspond to the case when λ_0 is reduced by a factor of two relative to those for the red curves. For this case, the CR intensity is lower at Earth and at the HP. We consider these two choices of λ_0 to correspond to solar minimum (red curves) and maximum (blue curves) modulation conditions. The intensity of CRs beyond the HP thus exhibits a solar cycle dependence, with $\sim$15% reduction at 100 MeV at the HP from solar minimum to maximum conditions.

For Figure 4, we investigate the curious feature that CR modulation in the outer heliosheath is independent on the magnitude of $\kappa_{||}$ in this region. The results are expressed in terms of the modulation fraction M, which is the CR intensity at the HP (at *V1*'s position) normalized to the LIS value at 100 MeV. Note that $M \leqslant 1$, where $M = 1$ corresponds to a *no-modulation* scenario. Moreover, the value of $1/M$ gives

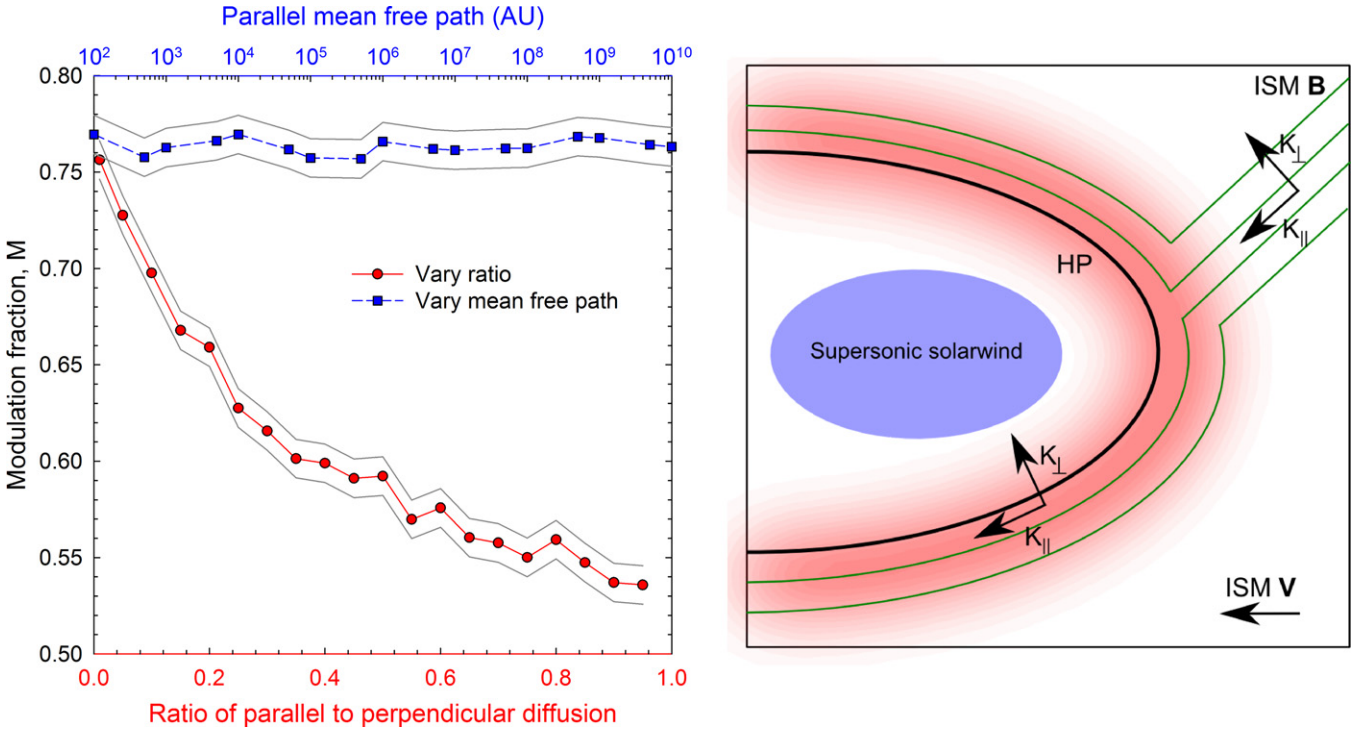

Figure 4. Left panel shows the CR intensity at 100 MeV, directly at the HP, normalized to LIS levels. The black squares are results when λ_0 in the outer heliosheath is changed, while $\eta = 0.02$ is kept constant. The red circles show the resulting intensity when η is changed, while $\lambda_0 = 10^5$ AU is held constant in the outer heliosphere. The gray lines show a 1% uncertainty in the results due to the stochastic nature of the numerical scheme, where 10,000 sample trajectories were solved. The right panel shows a schematic of the ISMF geometry close to the HP with an illustration of the parallel and perpendicular diffusive directions.

(A color version of this figure is available in the online journal.)

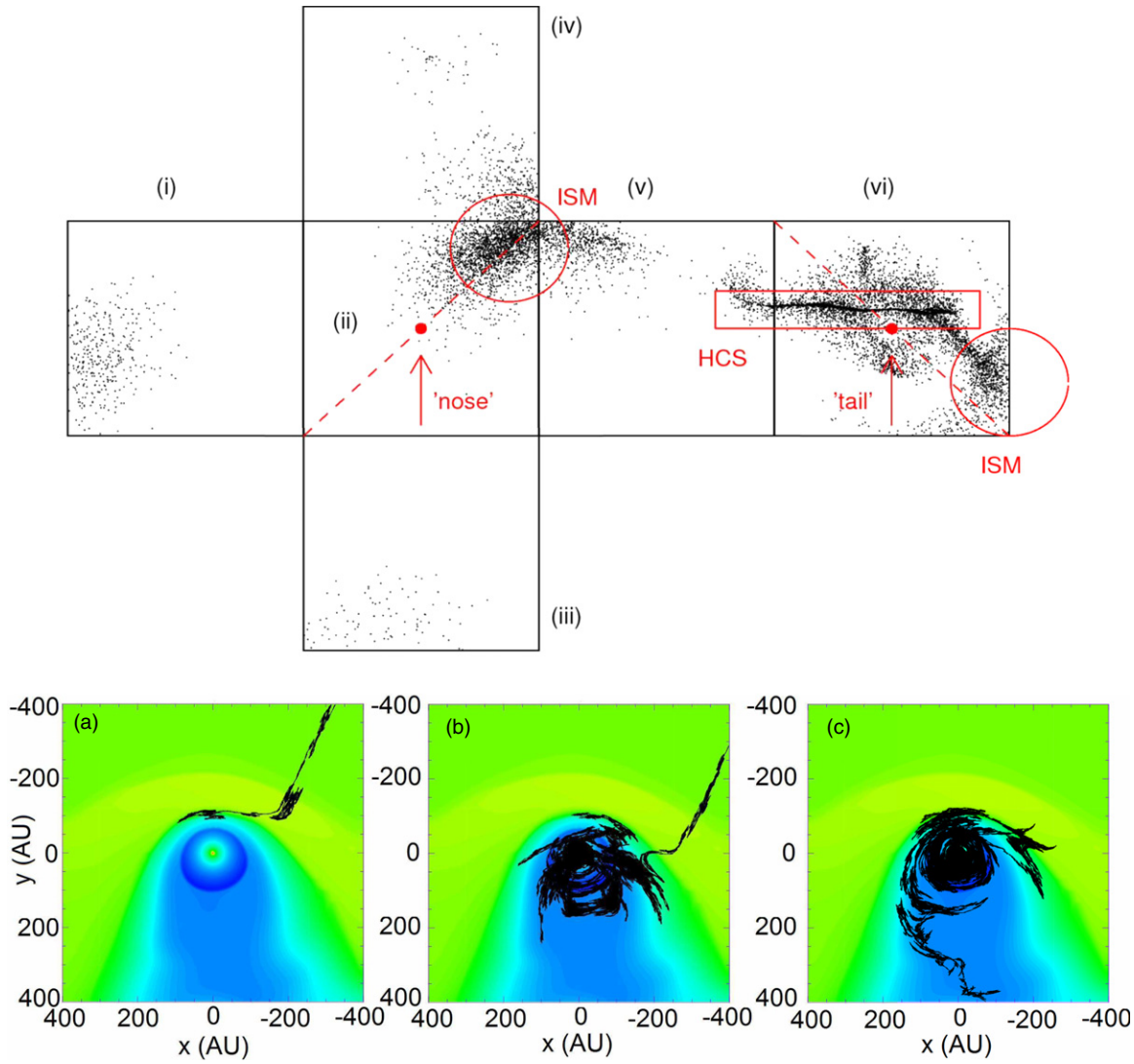

Figure 5. Top panel shows the position where CRs, with an energy of 100 MeV, enter the unfolded computational cube, before being *observed* at *V1*'s position at the HP. The bottom panel shows pseudo-particle traces, illustrating the behavior of CRs in the hybrid modeling approach, projected onto the ecliptic plane. The heliospheric geometry is shown here in terms of density with the ISM moving downward.

(A color version of this figure is available in the online journal.)

an indication of the level of modulation, i.e., a larger value of $1/M$ indicates more modulation (lower CR intensities). The black squares show the results when λ_0 is changed in the hybrid model, while $\eta = 0.02$ is kept constant. It is clear that M is independent of these changes. The red circles show the results when η is changed, while $\lambda_0 = 10^5$ AU is kept constant. For this scenario a strong dependence of M is found. The right panel of Figure 4 further explains this result: from the MHD computations shown in the previous section it is clear that the ISMF lines close to the HP are draped across the HP surface, so that they are essentially parallel to the HP. For CRs to enter the heliosphere and be modulated, they thus have to diffuse perpendicular to the ISMF lines. If they are unable to do this, no modulation will be observed in this region irrespective of the value of $\kappa_{||}$. The dependence on η can be summarized as

$$\frac{1}{M} \propto \kappa_{\perp}\tau. \tag{8}$$

The amount of modulation should be proportional to both τ (the time CRs spend close to the HP; the red shaded part in the figure) and $\kappa_{\perp}$ (noting again that CRs can only enter the HP by cross-field diffusion). Furthermore, with $\tau \propto 1/\kappa_{||}$ if $\kappa_{\perp} \ll \kappa_{||}$ (Strauss et al. 2011b), and $\kappa_{\perp} = \eta\kappa_{||}$, it is found that

$$M \propto \frac{1}{\eta}, \tag{9}$$

which is approximately the behavior evident in Figure 4.

The top panel of Figure 5 shows the position at the sides (boundaries) of the computational cube, where CRs with an energy of 100 MeV enter the computational volume in order to reach the position of the *V1* spacecraft at the HP. The computational cube is unfolded so that panel (ii) corresponds to the ISM inflow direction and panel (vi) to the tail region. The red circles show regions where the ISMF lines that connect with the position of *V1* just beyond the HP pierce the computational boundary. The red dashed lines show a projection of the undisturbed ISMF. A significant fraction of the CRs, reaching *V1*'s position at the HP, enters from the heliospheric tail regions (the red rectangle). This can be understood by

noting, from Figure 1, that the HMF spiral is stretched far out in the tail regions of the heliosphere (while being compressed in the nose regions), allowing effective parallel diffusion of CRs from the tail to the nose regions of the heliosphere. The bottom panel of Figure 5 shows pseudo-particle traces (projected onto the ecliptic plane), illustrating the behavior of CRs discussed above: case (a) shows CRs diffusing efficiently from the ISM to *V1*'s position at the HP, undergoing almost no modulation—the classical no-modulation paradigm. Case (b) shows a similar scenario, but with CRs entering the heliosphere, undergoing modulation (especially energy losses) after escaping the heliosphere before being *observed* at the HP. Case (c) shows CRs entering the tail regions of the heliosphere before propagating to the nose regions.

4. DISCUSSION AND CONCLUSIONS

A new hybrid CR modulation model is introduced, where the TPE is solved using a MHD simulated heliospheric environment instead of assuming a pre-described simplistic heliospheric geometry. The model is applied to CR modulation beyond the HP and selected results are presented for this Letter. The modeling results suggest that galactic CR modulation continues beyond the HP, so that *V1* will continue to measure a small but positive CR gradient well into the outer heliosheath. Moreover, it is shown that CR modulation in this region may exhibit measurable solar-cycle-related changes, due to variations in CR transport conditions within the HP. Due to the draping of ISMF lines across the HP, we show that CR transport beyond the HP is described mainly by the ratio of parallel to perpendicular transport.

The hybrid model, in its present form, contains various assumptions and simplifications, partly due to numerical constraints. We believe that qualitatively none of our results and conclusions would change when these simplifications are relaxed. For completeness sake, several possible future extensions (or modifications) of the hybrid model are discussed below that might affect the presented results quantitatively. We are confident in stating that they can be considered to cause second-order modulation effects. Including additional plasma/neutral species into the MHD model can change the dimensions of the heliospheric environment. It may also change the structure of the TS, but not to the extent that the modulation effect reported here can disappear. Acceleration of galactic CRs at the TS, and possibly through other mechanisms such as magnetic reconnection (e.g., Drake et al. 2010) near the HP, is improbable. The presence of a bow shock (BS; McComas et al. 2012) is not a prerequisite for the CR modulation effect presented here as CR transport is predominantly determined by the diffusion and other transport coefficients and not particular heliospheric structures. A theoretically founded model for the diffusion coefficients in the heliosheath is lacking although recent progress have been made (Zank et al. 2011). It is also unclear if instabilities at the HP, and possibly the BS if it exists, would affect the diffusion coefficients significantly enough to change CR modulation as presented here.

R.D.S., M.S.P., and S.E.S.F. are grateful for partial financial support provided by the South African National Research Foundation (NRF). K.S. and H.F. acknowledge support from the Deutsche Forschungsgemeinschaft (DFG) via the grants FI 706/9-1 and FI 706/16-1. The authors thank the Centre for High Performance Computing (www.chpc.ac.za) for computational resources and the VAPOR visualization platform (www.vapor.ucar.edu) for the free use of their rendering software. We also thank Frederic Effenberger for valuable comments.

REFERENCES

Achterberg, A., & Schure, K. M. 2011, MNRAS, 411, 2628
Ball, B., Zhang, M., Rassoul, H., & Linde, T. 2005, ApJ, 634, 1116
Brackbill, J. U., & Barnes, D. C. 1980, JCoPh, 35, 426
Drake, J. F., Opher, M., Swisdak, M., & Chamoun, J. N. 2010, ApJ, 709, 963
Effenberger, F., Fichtner, H., Scherer, K., et al. 2012, ApJ, 750, 108
Evans, C. R., & Hawley, J. F. 1988, ApJ, 332, 659
Florinski, V., & Pogorelov, N. V. 2009, ApJ, 701, 642
Gardiner, C. W. 1983, Handbook of Stochastic Methods (Germany: Springer)
Herbst, K., Heber, B., Kopp, A., Sternal, O., & Steinhilber, F. 2012, ApJ, 761, 17
Jin, S., & Xin, Z. 1995, Comm. Pure and Applied Math., 48, 235
Jokipii, J. R. 2001, in The Outer Heliosphere: The Next Frontiers, COSPAR Colliquia Series, Vol. 11, ed. K. Scherer, H. Fichtner, H. J. Fahr, & E. Marsch (New York: Pergamon Press), 227
Kloeden, P. E., & Platen, E. 1999, Numerical Solution of Stochastic Differential Equations (Germany: Springer)
Kopp, A., Büsching, I., Strauss, R. D., & Potgieter, M. S. 2012, CoPhC, 183, 530
Krülls, W. M., & Achterberg, A. 1994, A&A, 286, 314
Landau, L. D., & Lifshitz, E. M. 1984, Electrodynamics of Continuous Media (Sao Paulo: Pergamon Press)
McComas, D. C., & Schwadron, N. A. 2012, ApJ, 758, 19
McComas, D. J., Alexashov, D., Bzowski, M., et al. 2012, Sci, 336, 1291
McComas, D. J., Allegrini, F., Bochsler, P., et al. 2009, Sci, 326, 959
Moskalenko, I. V., Strong, A. W., Ormes, J. F., & Potgieter, M. S. 2002, ApJ, 565, 280
Müller, H.-R., Florinski, V., Heerikhuisen, J., et al. 2008, A&A, 491, 43
Opher, M., Stone, E. C., & Liewer, P. C. 2006, ApJL, 640, L71
Parker, E. N. 1958, ApJ, 128, 664
Parker, E. N. 1965, P&SS, 13, 9
Pen, U. L., Arras, P., & Wong, S. 2003, ApJS, 149, 447
Pogorelov, N. V., Heerikhuisen, J., Zank, G. P., et al. 2011, ApJ, 742, 104
Pogorelov, N. V., Stone, E. C., Florinski, V., & Zank, G. P. 2007, ApJ, 668, 611
Potgieter, M. S. 2008, AdSpR, 41, 245
Scherer, K., Fichtner, H., Strauss, R. D., et al. 2011, ApJ, 735, 128
Schwadron, N. A., Allegrini, F., Bzowski, M., et al. 2011, ApJ, 731, 56
Shalchi, A., & Büsching, I. 2010, ApJ, 725, 2110
Strauss, R. D., Potgieter, M. S., Büsching, I., & Kopp, A. 2011a, ApJ, 735, 83
Strauss, R. D., Potgieter, M. S., Kopp, A., & Büsching, I. 2011b, JGR, 116, A12105
Teufel, A., & Schlickeiser, R. 2003, A&A, 397, 15
Webber, W. R., McDonald, F. B., Cummings, A. C., et al. 2012, arXiv:1212.0883
Zank, G. P., Dosch, A., Hunana, P., et al. 2012, ApJ, 745, 35
Zhang, M. 1999, ApJ, 512, 409